Experimental analysis and mathematical modeling of fracture in RC elements with any aspect ratio

Maria Elena Perdomo, Ricardo Picon, Maria Eugenia Marante, François Hild, Stéphane Roux, Julio Florez-Lopez

EXPERIMENTAL ANALYSIS AND MATHEMATICAL MODELING OF FRACTURE IN RC ELEMENTS WITH ANY ASPECT RATIO

María Elena Perdomo[1,2], Ricardo Picón[2], María Eugenia Marante[2,*], François Hild[3], Stephan Roux[3], Julio Flórez-López[1]

1. Department of Structural Engineering, University of Los Andes, Mérida, Venezuela
2. Laboratory of Structural Mechanics, Lisandro Alvarado University, Barquisimeto, Venezuela
3. Laboratoire de Mécanique et Technologie (LMT) ENS Cachan / CNRS / UPMC / PRES UniverSud Paris, Cachan, France

ABSTRACT

In this paper, it is proposed a new model of the behavior of elements of arbitrary aspect ratio. The model allows for the analysis of large and complex structures and it is based on concepts of classic fracture mechanics and continuum damage mechanics. The model considers independent variables that measure the degree of shear and flexural damage separately.

This paper also presents an experimental analysis of the behavior of RC elements with the use of digital image correlation technique which allows for the classification and quantification of the different failure mechanisms in a much better way than the classic procedures.

Keywords: Reinforced Concrete Elements, Experimental Analysis, Numerical Analysis, Shear Damage, Flexural Damage, Damage Mechanics.

**Corresponding author: Telefax: +58 251 2592173, email: emarante@ucla.edu.ve, postal address:* Prolong. Av. La Salle, Decanato de Ingeniería Civil, Lisandro Alvarado University, Barquisimeto, Estado Lara, Venezuela.

1. INTRODUCTION

Real RC structures present components of very diverse nature. Including all of them in the analyses is essential for realistic numerical simulations of severe nonlinear behavior such as in cases of earthquake loading, displacement of supports, impacts or explosions. One of the most difficult aspects is the modeling of structural elements with arbitrary aspect ratios; this is however a fundamental issue. Dual systems are often used as a good structural alternative for buildings and facilities in earthquake-prone areas; this kind of structures combines frames with short elements and walls. Even in framed structures, short or intermediate columns and beams may appear as a result of inadequate disposition of masonry walls or other non-structural components.

The models for RC components subjected to bending using plastic hinges or distributed plasticity are the most abundant, models for walls and squat elements with bending and shear are less numerous but still there is a large choice of options (some of the most recent are [1-4]).

The goal of this work is to propose a new model of the behavior of elements of arbitrary aspect ratio within the framework of the classic analysis of structures. The model is based on concepts of classic fracture mechanics and continuum damage mechanics. Many other models are also included within the latter sub-field, but they are limited to slender elements only [5-12], or walls exclusively [13-14].

This paper also presents an experimental analysis of the behavior of RC elements. Experimental analyses aim for the determination of the resistance and deformation capacity in order to predict the inelastic response of slender elements or walls (see for instance [15-17). These studies show that for beams and columns of large aspect ratios the most important effect is bending but with its reduction, shear stresses become progressively more important and may be the dominant failure mechanism.

The experimental study presented in this paper differs from the aforementioned references in the use of digital image correlation (DIC), see for instance [18]. This method allows for the classification and quantification of the different failure mechanisms in a much better way than the classic procedures, which are either local or performed by visual inspection.

2. EXPERIMENTAL ANALYSIS

The experimental analysis [19] was carried out using DIC. In this method the specimens to be tested are marked randomly using dark paint dots. A first digital photo of reference is taken before the test. Next, further pictures are taken during the experiment while the chosen external forces are applied. A computer program [18] processes first the reference digital image; the program divides this photo into small portions that may be imagined as small "finger prints" and identifies each of them. Then, the program analyses the following picture, looks for the same "finger prints" and determines their new position in the picture. This procedure gives the average displacement vector of each specific portion. Next, the program feeds a finite element mesh with those displacements. In this way the displacement field of the specimen is measured. Notice that the nodal displacements are experimentally measured and not mathematically computed. The same procedure is followed sequentially with each digital photo of the test. With the displacement FE field, the program computes the strain field using the conventional techniques. Cracks in concrete appear as concentrations of strains. For instance, Fig. 2 shows diagonal tension cracks and/or flexure cracks in beams. Notice that the program also provides for an automatic and objective quantification (independent of the observer) of the intensity of cracking.

The first series of tests was designed to show and quantify the modifications of the cracking patterns with the aspect ratio. Three specimens that represent RC beams in cantilever with different aspect ratios were tested (see Fig. 1). The properties of these specimens can be found in [19]. The variation of the aspect ratio was achieved using identical specimens but changing the position of the lateral force. Specimen B4 is a slender beam with an aspect ratio of 7.11; specimens B2 and B3 represent intermediate beams with, respectively, aspect ratios of 3.56 and 5.36 [19]. The loading history is shown in Fig. 1b. It is cyclic and displacement-controlled in the loading phase with increasing maximum displacements after each cycle; the

unloading phase is load-controlled and the final force at the end of each cycle is always zero. This kind of test is denoted in this paper “mono-sign” since both, displacements and forces are cyclic but never change sign.

Fig. 1

Fig. 1 a) Beams with different aspect ratios b) Loading history

The cracking patterns obtained with DIC are shown in Fig. 2. As expected, concrete cracks in beam B4 are concentrated in the plastic hinge zone and appear to be flexure cracks. The intermediate beams exhibit mixed cracking patterns. The transition from flexure to shear cracking with the aspect ratio appears to be progressive.

Fig. 2

Fig. 2 Cracking patterns revealed by DIC in beams with different aspect ratios

Several RC walls with different aspect ratios [19] were also tested with mono-sign loadings; in this paper, the results of only one of them (see Fig. 3) are shown in Fig. 4. In that case, dominant shear cracks appear in the specimen. The longitudinal reinforcement of this wall was over-dimensioned in order to minimize as much as possible flexure damage.

Fig. 3

Fig. 3 RC wall

Fig. 4

Fig. 4 Cracking pattern in a wall revealed by DIC

It was observed [19] that the presence of an axial force on the specimens does not modify significantly the cracking pattern; it just alters slightly the orientation of the shear cracks.

3. SIMPLIFIED MODELING OF FRACTURE USING INTERNAL VARIABLES

Consider a RC structure composed of *n* nodes and *m* elements of any aspect ratio. A node *i* of the structure has three degrees of freedom: the displacements u_i and w_i in the directions of the global axis X and Z and the rotation θ_i. The generalized deformations of an element *b* between nodes *i* and *j* are represented by the matrix $\{\mathbf{\Phi}\}_b^t = (\phi_i^b, \phi_j^b, \delta_b)$ .The terms ϕ_i^b and ϕ_j^b are the relative rotations of the element end-sections with respect to the cord and δ_b is the elongation (see Fig. 5a). The generalized stress matrix is denoted $\{\mathbf{M}\}_b^t = (m_i^b, m_j^b, n_b)$ and includes the bending moments at the end sections and the axial force (see Fig. 5b). If the forces distributed on the element are small with respect to the nodal forces, then the shear force is approximately constant and can be computed as:

$$v_i \cong v_j \cong V_b = \frac{m_i^b + m_j^b}{L_b} \tag{1}$$

Fig. 5

Fig. 5 a) Generalized deformations b) Generalized stresses

The experimental analysis showed that RC elements with arbitrary aspect ratio may have flexural cracks in the plastic hinge zone and/or shear cracks along the element. A simplified representation of the fracture process is obtained using the damage variables indicated in Fig. 6. Those parameters take values between zero and one as in continuum damage mechanics [20] but, in the present case, they represent densities of macro-cracks instead of micro-defects. Flexural damage may be lumped at the plastic hinges [5]; the flexural damage matrix

$(\mathbf{D})_b = (d_i, d_j)$ includes those damage variables. It is proposed the introduction of a new damage variable d_s that accounts for shear damage. It is important to underline that, at least in the case of flexural damage; these values can be related to the possibility of repair of the element.

Fig. 6

Fig. 6 Flexure and shear damage variables

Finally, there are two main sources of possible plastic deformations in the elements. The first one is related to the yielding of longitudinal reinforcement. Conventionally, these plastic deformations are represented as rotations of the plastic hinges that may be grouped into the generalized plastic deformation matrix: $\{\mathbf{\Phi}^p\}_b^t = (\phi_i^p, \phi_j^p, 0)$, see Fig. 7a; permanent elongations of the cord are neglected.

The second mechanism is related to the yielding of the transverse reinforcement that produces plastic distortions. They may be represented by the plastic distortion matrix $\{\boldsymbol{\gamma}^p\}_b^t = (\gamma^p, \gamma^p, 0)$, see Fig. 7b [13].

Fig. 7

Fig. 7 Plastic deformations in a RC element a) Plastic rotation b) Plastic distortion

4. CONSTITUTIVE EQUATIONS: STATE LAW

Constitutive laws in classic continuum damage mechanics are based on two simple but very powerful concepts: the effective stress $\bar{\sigma}$ and the hypothesis of equivalence in deformations [20]:

$$\bar{\sigma} = \frac{\sigma}{1-\omega}; \qquad \bar{\sigma} = \mathrm{E}(\varepsilon - \varepsilon^{\mathrm{p}}) \qquad \Rightarrow \qquad \sigma = (1-\omega)\mathrm{E}(\varepsilon - \varepsilon^{\mathrm{p}}) \tag{2}$$

where ω is the dimensionless continuum damage variable taking values between zero and one. Instead of writing the state law in terms of stiffness as in Eq. (2c), it is better for the purpose of this paper to express it in terms of flexibility:

$$\varepsilon - \varepsilon^{p} = \frac{1}{(1-\omega)E}\sigma \Rightarrow \varepsilon = \varepsilon^{e} + \varepsilon^{\mathrm{d}} + \varepsilon^{\mathrm{p}} \quad \text{where} \quad \varepsilon^{e} = \frac{1}{E}\sigma; \ \text{and} \quad \varepsilon^{d} = \frac{\omega}{E(1-\omega)}\sigma \tag{3}$$

Notice that the term ε^{e} is an elastic strain, ε^{p} is the plastic strain and ε^{d} can be interpreted as an additional damage-related one. Correspondingly, there is an initial elastic flexibility $1/E$ and a damage-related one: $\omega/E(1-\omega)$. If damage is equal to zero, the damage strain is zero too; if damage tends to one, the damage-related flexibility and deformation tend to infinity. Notice the existence of three strain terms for the three phenomena under consideration: elasticity, damage and plasticity.

Return to the case of RC elements. In the previous section, five main phenomena were identified; thus, according to the hypothesis of equivalence in deformations, total deformation

is decomposed into five terms: an elastic deformation, a shear damage term, a flexural damage one, the plastic distortion matrix and the plastic hinge rotation matrix:

$$\{\mathbf{\Phi}\}_{\mathrm{b}} = \{\mathbf{\Phi}^{\mathrm{e}}\}_{\mathrm{b}} + \{\boldsymbol{\gamma}^{\mathrm{d}}\}_{\mathrm{b}} + \{\mathbf{\Phi}^{\mathrm{d}}\}_{\mathrm{b}} + \{\boldsymbol{\gamma}^{\mathrm{p}}\}_{\mathrm{b}} + \{\mathbf{\Phi}^{\mathrm{p}}\}_{\mathrm{b}} \tag{4}$$

The elastic deformations may be written as a function of stresses using the conventional flexibility matrices:

$$\{\mathbf{\Phi}^{\mathrm{e}}\}_{\mathrm{b}} = [\mathbf{F}_0]_{\mathrm{b}}\{\mathbf{M}\}_{\mathrm{b}} \text{ ; where } \left[\mathbf{F}_o\right]_b = \begin{bmatrix} \frac{L_b}{3EI_b} & -\frac{L_b}{6EI_b} & 0 \\ -\frac{L_b}{6EI_b} & \frac{L_b}{3EI_b} & 0 \\ 0 & 0 & \frac{L_b}{EA_b} \end{bmatrix} + \begin{bmatrix} \frac{1}{GA_bL_b} & \frac{1}{GA_bL_b} & 0 \\ \frac{1}{GA_bL_b} & \frac{1}{GA_bL_b} & 0 \\ 0 & 0 & 0 \end{bmatrix} \tag{5}$$

The first part of $[\mathbf{F}_0]_b$ is the Bernoulli elastic flexibility matrix and the second term is the Timoshenko elastic flexibility matrix. The parameters EI_b and GA_b are the usual rigidities to, respectively, bending and shear of the element.

The third deformation term in Eq. (4) can be written, according to the hypothesis of equivalence in deformation, as:

$$\{\boldsymbol{\gamma}^{\mathrm{d}}\}_{\mathrm{b}} = [\mathbf{C}_{\mathrm{s}}(\mathrm{d}_{\mathrm{s}})]_{\mathrm{b}}\{\mathbf{M}\}_{\mathrm{b}} \qquad \text{where} \qquad \left[\mathbf{C}_s(d_s)\right] = \frac{d_s}{1-d_s}\begin{bmatrix} \frac{1}{GA_bL_b} & \frac{1}{GA_bL_b} & 0 \\ \frac{1}{GA_bL_b} & \frac{1}{GA_bL_b} & 0 \\ 0 & 0 & 0 \end{bmatrix} \tag{6}$$

Notice that if the shear damage is zero then the damage deformations are also zero. If the shear damage tends to one, the Timoshenko flexibility tends to infinity.

Similarly, the fourth term of Eq (4) is:

$$\{\mathbf{\Phi}^d\}_b = [\mathbf{C}_f(\mathbf{D})]_b \{\mathbf{M}\}_b \qquad \text{where} \quad [\mathbf{C}_f(\mathbf{D})]_b = \begin{bmatrix} \frac{d_i}{1-d_i}\frac{L_b}{3EI_b} & 0 & 0 \\ 0 & \frac{d_j}{1-d_j}\frac{L_b}{3EI_b} & 0 \\ 0 & 0 & 0 \end{bmatrix} \tag{7}$$

This time, the Bernoulli flexibility terms tend to infinity when the damages tend to one. The combination of (4-7) gives the state law of a RC element:

$$\{\mathbf{\Phi} - \mathbf{\Phi}^p - \boldsymbol{\gamma}^p\}_b = \left[\mathbf{F}(\mathbf{D}, d_s)\right]\{\mathbf{M}\}_{\mathrm{b}} \tag{8}$$

$$\left[\mathbf{F}(\mathbf{D}, d_s)\right] = \begin{bmatrix} \frac{L_b}{3EI_b(1-d_i)} + \frac{1}{GA_bL_b(1-d_s)} & -\frac{L_b}{6EI_b} + \frac{1}{GA_bL_b(1-d_s)} & 0 \\ -\frac{L_b}{6EI_b} + \frac{1}{GA_bL_b(1-d_s)} & \frac{L_b}{3EI_b(1-d_j)} + \frac{1}{GA_bL_b(1-d_s)} & 0 \\ 0 & 0 & \frac{L_b}{EA_b} \end{bmatrix}$$

The local stiffness matrix is, of course, the inverse of $\left[\mathbf{F}(\mathbf{D}, d_s)\right]$ and its computation is immediate using any symbolic manipulation program but the resulting expression is too complex to be read easily.

5. GENERALIZED GRIFFITH CRITERIA

The theory of linear elastic fracture mechanics states that crack propagation is only possible if the energy stored in the structure is sufficient to overcome the fracture energy of the material. The same Griffith balance energy can be used in the present case. The complementary deformation energy W_b of the element can be computed from the state law (8):

$$W_b = \frac{1}{2}\{\mathbf{M}\}_b^t\{\mathbf{\Phi} - \mathbf{\Phi}^p - \boldsymbol{\gamma}^p\}_b = \frac{1}{2}\{\mathbf{M}\}_b^t[\mathbf{F}(\mathbf{D}, d_s)]_b\{\mathbf{M}\}_b \tag{9}$$

Assuming that the damage mechanisms are uncoupled, the energy release rate for shear damage G_s is:

$$G_s = \frac{\partial W_b}{\partial d_s} = \frac{L_b V_b^2}{2GA_b(1-d_s)^2} \tag{10}$$

Notice that this variable depends indeed on the shear force V_b . The use of a generalized form of the Griffith criterion allows for the computation of the shear-damage:

$$\begin{cases} \Delta d_s = 0 & \text{if } G_s < R_s \\ G_s = R_s & \text{if } \Delta d_s > 0 \end{cases} \tag{11}$$

where R_s is the shear damage resistance function and Δd_s represents increments of damage. This generalized form of the Griffith criterion was also discussed in [13].

The shear damage resistance R_s can be identified experimentally using the test on the wall described in Section 2. Fig. 8a shows the plot of deflection vs. lateral force obtained in that test. This test was chosen for the identification because the DIC analysis indicated very small, negligible, flexure damage. In this particular case, with the corresponding boundary conditions, the state law (8) becomes:

$$V = Z(d_s)(t - t_p); \qquad t_p = \gamma^p L; \qquad Z(d_s) = \frac{3EI\,GA(1-d_s)}{L(L^2GA - L^2GAd_s + 3EI)} \tag{12}$$

where *t* is the lateral displacement and V the lateral force. Notice that Eq.(12) corresponds to the straight lines represented in Fig. 8a.

Fig. 8

Fig. 8 a) Deflection vs. lateral force in a RC wall b) Shear energy release rate vs. shear damage

Therefore, the slopes *Z* may be measured in the test. Thus, an experimental value of shear damage can be determined for each unloading in the test using:

$$d_s = \frac{3GAEI - 3Z\,L\,EI - Z\,L^3GA}{GA(3EI - L^3Z)} \tag{13}$$

Notice that this is simply an extension of the elastic stiffness variation method well-known in fracture and continuum damage mechanics [20].

It is possible to plot shear damage against shear energy release rate (Fig. 8b) because experimental values of the latter variables can be obtained using Eq. (10). With this plot it is possible to propose the following expression for the crack resistance function:

$$R(d_s) = R_{0s} + q_s \frac{\ln(1-d_s)}{1-d_s} \tag{14}$$

Notice that there are an initial value of crack resistance R_{0s} and a logarithmic hardening term. The latter is due to the action of the reinforcement that obstructs shear cracks propagation. In practical applications, the parameters R_{0s} and q_s does not need to be measured experimentally; they may be determined from well-known concepts of the reinforced concrete theory as it is explained in the following paragraph.

Consider again the Griffith equation: $G_s = R_s$. This expression defines a general relationship between shear force and shear damage:

$$L_b V_b^2 = 2GA_b(1-d_s)^2\left(R_{0s} + q_s \frac{\ln(1-d_s)}{1-d_s}\right) \tag{15}$$

This equation gives the plot of damage vs. shear force indicated in Fig. 9.

Fig. 9

Fig. 9 Damage vs. shear force according to Griffith criterion

Notice that the values of the first cracking shear force V_{cr} and ultimate shear force V_u in Fig. 9 can be indeed computed using RC theory [21-22] with a reasonable accuracy. Those values enable for the computation of the parameters R_{0s} and q_s in the shear crack resistance function.

Flexure-damage can also be computed using the same procedure. The damage driving moments are:

$$G_i = \frac{\partial W_b}{\partial d_i} = \frac{L_b\, m_i^2}{6EI_b(1-d_i)^2}; \qquad G_j = \frac{\partial W_b}{\partial d_j} = \frac{L_b\, m_j^2}{6EI_b(1-d_j)^2} \tag{16}$$

Notice that these new energy release rates depend now on the flexural moments and not on the shear force. Similar generalized forms of the Griffith criterion can also be proposed and the corresponding flexure crack resistance function identified [5]. The same method of the variation of the elastic stiffness can also be adapted to the experimental measurement of flexure-damage [5] but in this case DIC technique is used to check that shear cracks are negligible. It is interesting to note that the flexure damage resistance function of a plastic hinge i may have the same general expression as Eq.(14) but, of course, with different values for the parameters:

$$R(d_i) = R_{0f} + q_f \frac{\ln(1-d_i)}{1-d_i} \tag{17}$$

It appears that the function Eq. (17), or (14), can be considered as a general expression for damage resistance in RC elements.

6. YIELD FUNCTIONS

The last components of the model are the yield functions needed for the computation of the plastic distortion and the plastic rotations. The starting point is the conventional yield functions with linear kinematic hardening; next, the hypothesis of equivalence in deformation is used again with the following effective shear force and effective flexural moment:

$$\overline{V} = \frac{V}{1-d_s} = \frac{m_i + m_j}{(1-d_s)L}\,; \qquad \text{and} \qquad \overline{m_i} = \frac{m_i}{1-d_i} \tag{18}$$

$$f_s = \left|\overline{V} - c_s\gamma^p\right| - k_{os} = \left|\frac{m_i + m_j}{(1-d_s)L} - c_s\gamma^p\right| - k_{os} \le 0\,; \qquad f_i = \left|\frac{m_i}{1-d_i} - c_i\phi_i^p\right| - k_{0i} \le 0 \tag{19}$$

where c_s, c_i, k_{oi} and k_{os} are, too, model parameters. All of them can also be computed using reinforced concrete theory [19].

The last expressions for a full analysis of RC structures are the kinematic and equilibrium equations. Both of them are exactly the same as those for the analysis of nonlinear elastic frames.

7. NUMERICAL VALIDATION OF THE MODEL

The model was included into the library of a well-known commercial structural analysis program [23] as a new finite element [19]; then, all the tests presented in Section 2 were simulated.

Fig. 10a-b shows the experimental results and numerical simulation of the slender column (specimen B4 of Figs. 1-2) in a plot of deflection vs. lateral force; note that the numerical results are very good. Fig. 10c indicates the histories of damage. The DIC analysis validates the large value of flexure damage (0.58) and negligible shear damage (0.03) obtained in the simulation.

Fig. 10

Fig. 10 Behavior of a slender RC beam in cantilever a) Experimental deflection vs. lateral force b) Numerical deflection vs. lateral force c) Damage evolution

Fig. 11b shows the numerical simulation of the longer intermediate beam (specimen B3 in Figs. 1-2). The results of the numerical simulation are also very good. The histories of damage are different (Fig. 11c); the final value of flexure damage is also very large (0.74) but now shear damage is not negligible (0.33). Again, this is in agreement with DIC observations (see specimen B3 in Fig.2).

Fig. 11

Fig. 11 Behavior of an intermediate RC beam in cantilever a) Experimental deflection vs. lateral force b) Numerical deflection vs. lateral force c) Damage evolution

The results for the shorter intermediate beam (specimen B2) are shown in Fig. 12. The numerical simulation is good and now the relationship between flexure damage and shear

damage are reversed, with final values of 0.47 and 0.85 respectively. This is again in good agreement with DIC results (see specimen B2 in Fig.2).

Fig. 12

Fig. 12 Behavior of an intermediate RC beam in cantilever a) Experimental deflection vs. lateral force b) Numerical deflection vs. lateral force c) Damage evolution

Fig. 13 shows the numerical simulations of the shear wall where shear-damage is the main mechanism of failure while flexure-damage is small or even negligible.

Fig. 13

Fig. 13 Behavior of a RC wall in cantilever a) Experimental deflection vs. lateral force b) Numerical deflection vs. lateral force c) Damage evolution

8. EXPERIMENTAL ANALYSIS AND NUMERICAL SIMULATION OF A TWO-ELEMENTS STRUCTURE

The last validation was carried out using the structure shown in Fig. 14a. This is a continuous beam of two elements, one short and one slender, separated by a chunk that represents a column; the beam is embedded at its ends in two heavy RC blocks that represent fixed supports. A mono-sign loading was applied at the column. The goal of this test is to reproduce the short element effect similar to the one shown in Fig. 14b, to test the ability of the model to simulate it and to recognize the different patterns of cracking in the structure.

Fig. 14

Fig. 14 a) Continuous two-element beam b) Failure of a short column in a RC structure [24]

As expected, the experimental results show moderate flexure damage in the plastic hinge regions of both elements and severe shear damage in the short beam. In this test, the DIC analysis was not carried out, the software was not available at that time.
The quality of the numerical simulation can be evaluated in the plots of deflection vs. force for the column shown in Fig. 15.

Fig. 15

Fig. 15 Deflection vs. force a) Experimental analysis b) Numerical simulation

The histories of damage obtained numerically are presented in Fig. 16. They can be compared with the cracking patterns observed in the test. Notice that the simulation is in good agreement with experimental values.

Fig. 16

Fig. 16 Cracking pattern in the continuous beam a) Short element and corresponding damage history b) Slender element and corresponding damage history

9. FINAL REMARKS AND CONCLUSIONS

In general terms, in the structural mechanics field, fracture mechanics theory is the only accepted tool to analyze damage due to crack propagation. It is clear now that the fundamental concepts of fracture and continuum damage mechanics can be adapted to the simplified analysis of RC structures with an adequate engineering accuracy and in a large variety of applications. Notice that, with the present model, a very large structure may be discretized conveniently in a few hundreds of elements at most; and only three damage parameters per element are enough for a quite thorough description of the state of fracture and deterioration of them; this description is appropriated for most practical applications. The required computational load represents a very low demand for actual finite element programs and computers.

The quantification in a separate way of shear and flexural damage is important for the structural vulnerability assessment since the corresponding failures exhibit different degrees of risk; it may be necessary to consider different tolerances in each case. This information can also be useful for retrofitting projects since the urgency and the reparation techniques are different in each case.

It must be underlined the great potential that DIC offers for the development of new methods in the analysis and design of RC structures. The results presented in this paper are just a small example of a large spectrum of possibilities. This technique allows not only for an objective and automatic determination of fracture patterns but also for its quantification. This feature was very important for the validation of the computed values of damage.

10. ACKNOWLEDGMENT

The results presented in this paper were obtained in the course of an investigation sponsored by FONACIT (G-2001001210, PI-2005000762) and CDCHT-UCLA (002-IC-2005).

11. REFERENCES

[1] D'Ambrisi A, Filippou FC. Modeling of cyclic shear behavior in RC members. J Struct Eng 1999; 125(10):1143-50.

[2] Miao ZW, Lu XZ, Jiang JJ and Ye LP. Nonlinear FE Model for RC Shear Walls Based on Multi-layer Shell Element and Microplane Constitutive Model. Comput Meth Eng and Sci 2006; EPMESC X, Aug. 21-23, Sanya, Hainan,China.

[3] Mohr, S., Bairán J. and Marí, A. A frame element model for the analysis of reinforced concrete structures under shear and bending. Eng Struct, Elsevier Science 2010; 32: 3936-54.

[4] Mergos, P.E. and Kappos, A.J. A distributed shear and flexural flexibility model with shear-flexural interaction for R/C members subjected to seismic loading. Earthq Eng Struct Dyn 2008; 37: 1349–70.

[5] Cipollina A, López-Inojosa A, Flórez-López J. A simplified damage mechanics approach to nonlinear analysis of frames. Comput Struct 1995; 54 (6): 1113-26.

[6] Perera R, Carnicero A, Alarcon E. A fatigue damage model for seismic response of RC structures. Comput Struct 2000; 78(1-3): 293-302.

[7] Kaewkulchai G, Williamson EB. Beam element formulation and solution procedure for dynamic progressive collapse analysis. Comput Struct 2004; 82(7-8): 639-51.

[8] Valipour H, Foster S. Nonlocal damage formulation for a flexibility-based frame element. J Struct Eng ASCE 2009; 135(10): 1213-21.

[9] Rahasankar J, Iyer N, Prasad M. Modelling inelastic hinges using CDM for nonlinear analysis of reinforced concrete frame structures. Comput Conc 2009; 6(4): 319-41.

[10] Sisniegas G, Homce AL. Application of lumped dissipation model in nonlinear analysis of reinforced concrete structures. Eng Struct 2010; 32(4): 974-81.

[11] Faleiro J, Oller S, Barbat A. Plastic-damage analysis of reinforced concrete frames. Eng Comput 2010; 27(1-2): 57-83.

[12] De Araujo F, Baroncini S. Application of a lumped dissipation model to reinforced concrete structures with the consideration of residual strains and cycles of hysteresis. J Mech Mat Struct 2008; 3(5): 1011-31.

[13] Thomson E, Perdomo ME, Picón R, Marante ME, Flórez López J. Simplified model for damage in squat RC shear wall. Eng Struct 2009; 31 (10), 2215-23.

[14] Hua-Jing Z, Xing-Wen L. Plastic-damage model for reinforced concrete shear walls. Innov. Sustain Struct 2009; 1-2: 404-09.

[15] Greifenhagen C, Lestuzzi P. Static cyclic test on lightly reinforced concrete shear walls. Eng Struct 2005; (27):1703-12.

[16] Güray A. Shear strength of reinforced concrete beams with stirrups. Mat and Struct 2008; 41: 113–122.

[17] Sezen H and Moehle JP. Seismic test of concrete columns with light transverse reinforcement. ACI Struct J 2007; 133(11): 864-70.

[18] Besnard G, Hild F, Roux S. Finite-element displacement fields analysis from digital images: application to Portevin–Le Châtelier bands. Exp Mech 2006; 46: 789–803.

[19] Perdomo ME. Fractura y Daño en Estructuras Duales de Concreto Armado, Doctoral Thesis, University of Los Andes, Venezuela, 2010.

[20] Lemaitre J, Chaboche JL. Mechanics of Solids Materials, Dunod, Paris, 1988.

[21] American Concrete Institute 2005. Building code requirement for structural concrete. ACI Committee 318, Farmington Hills, Mich.

[22] Sezen H and Moehle JP. Seismic behavior and modeling of reinforced concrete building columns. J Struct Eng ASCE 2004; 130(1): 1692-1703.

[23] Abaqus user's manual – Version 6.2. Pawtucket, RI: Hibbitt, Karlson & Sorensen, Inc, 2001.

[24] DRM Library, World Institute for Disaster Risk Management. September 23 2011. <http://www.drmonline.net/drmlibrary/peru_photos.htm>.

Figure

Click here to download high resolution image

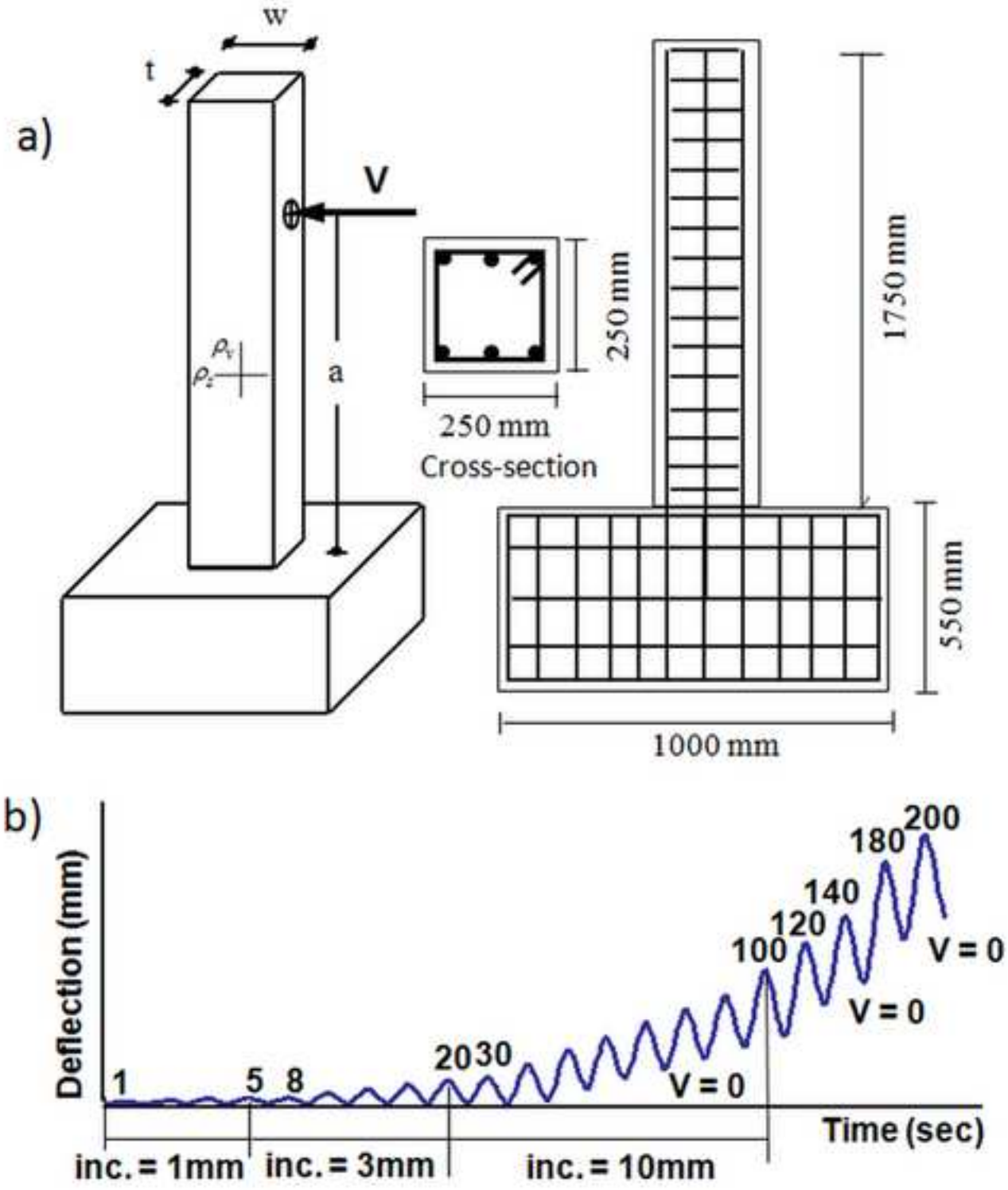

Figure
Click here to download high resolution image

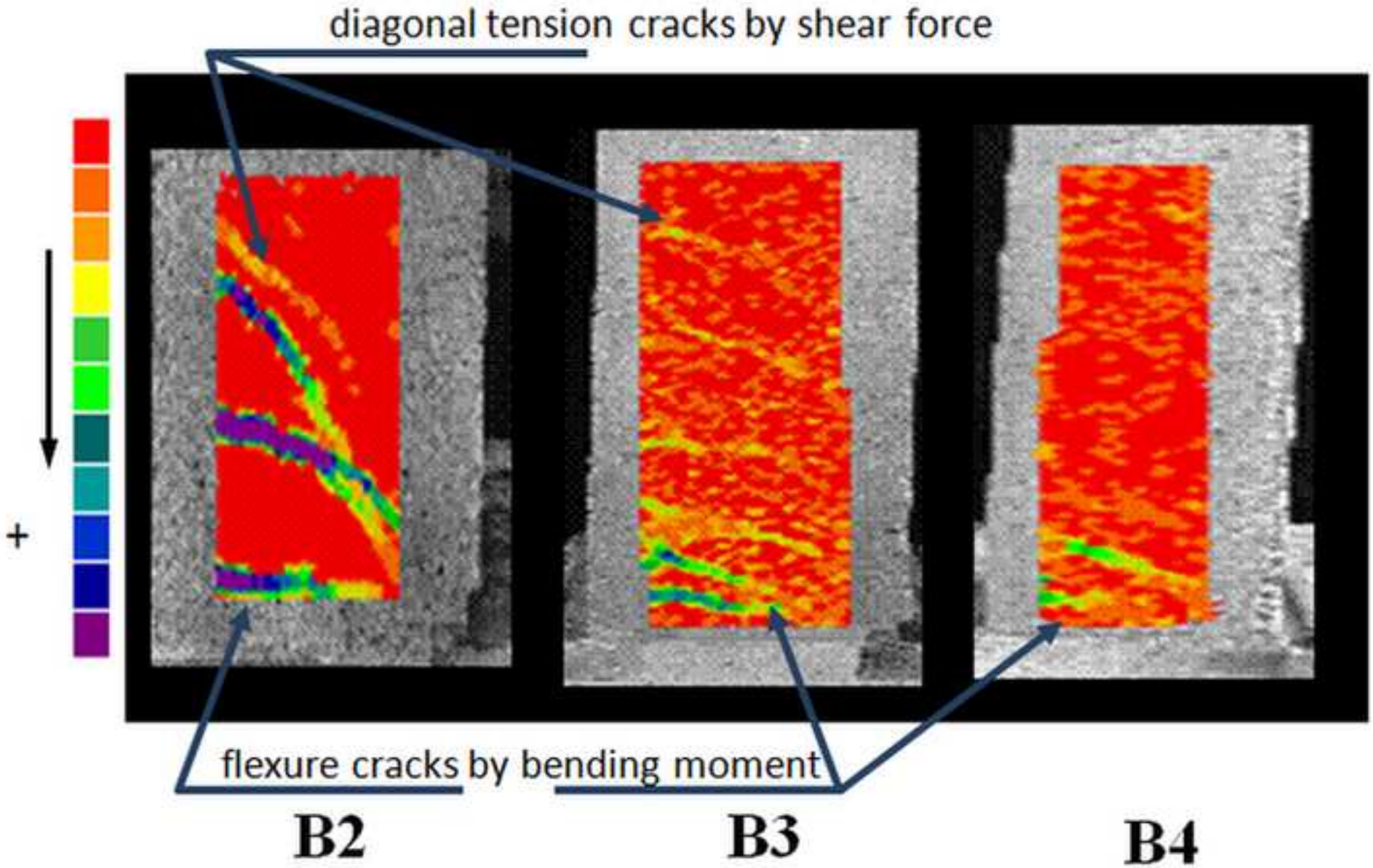

Figure

Click here to download high resolution image

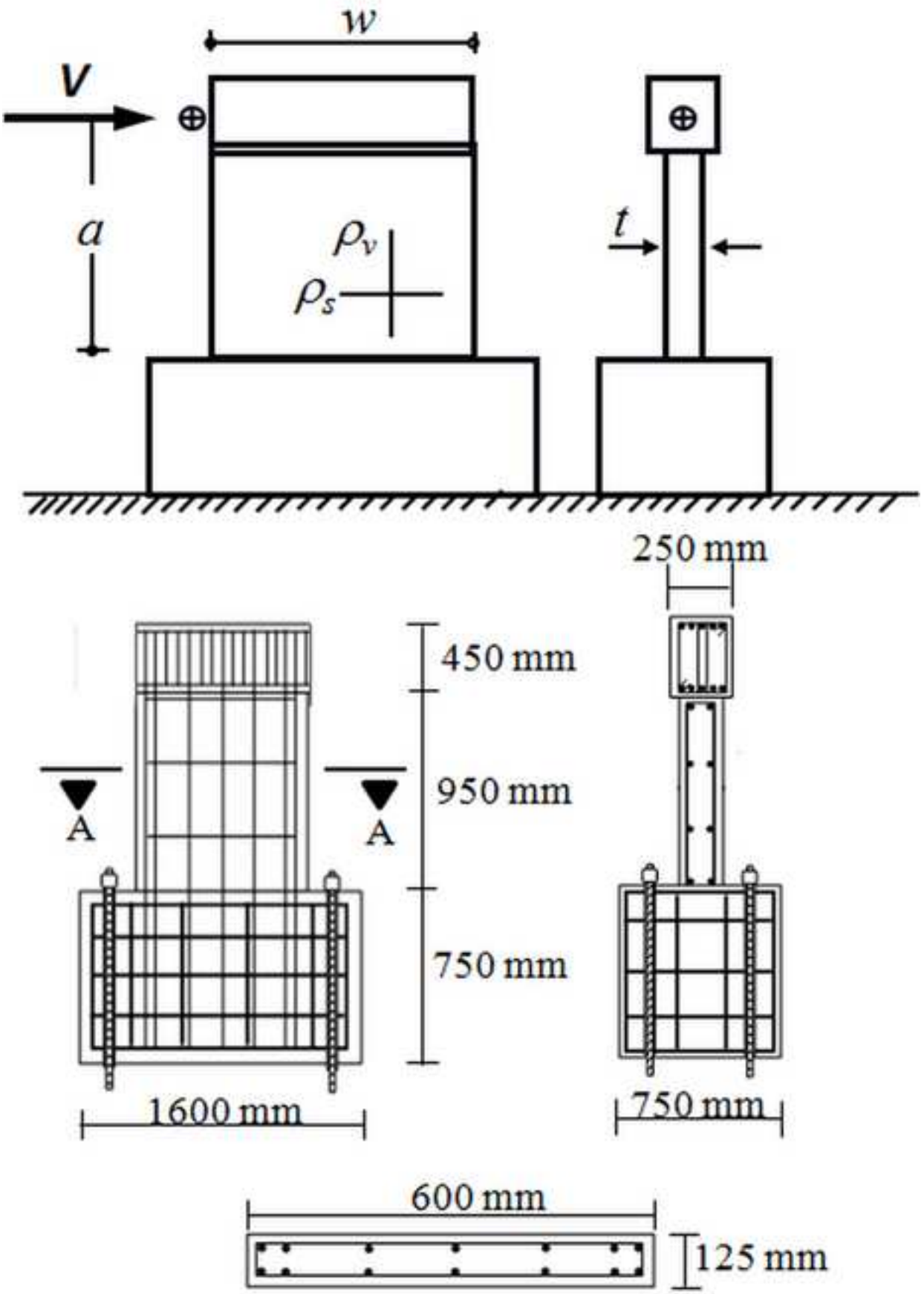

Section A-A

Figure
Click here to download high resolution image

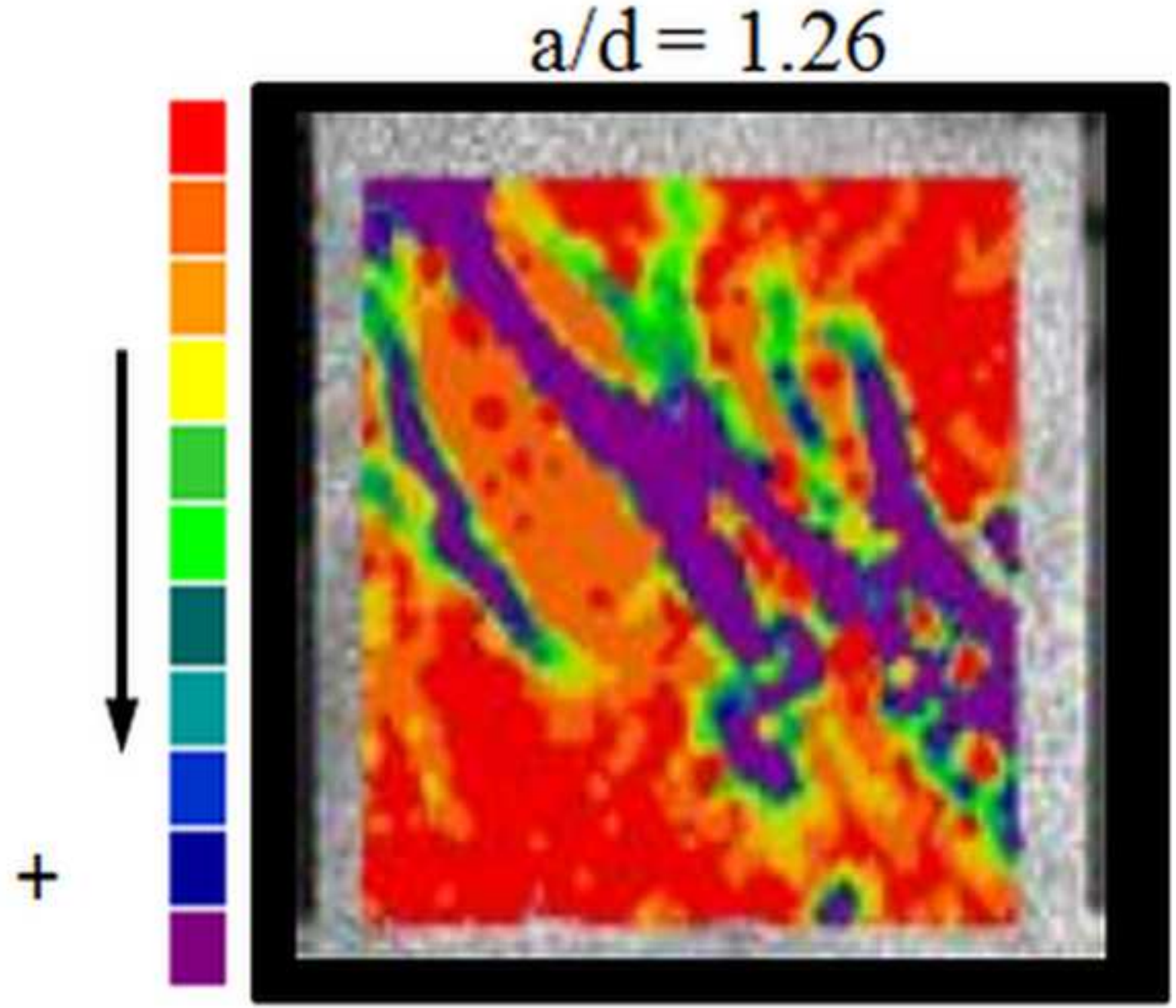

Figure
Click here to download high resolution image

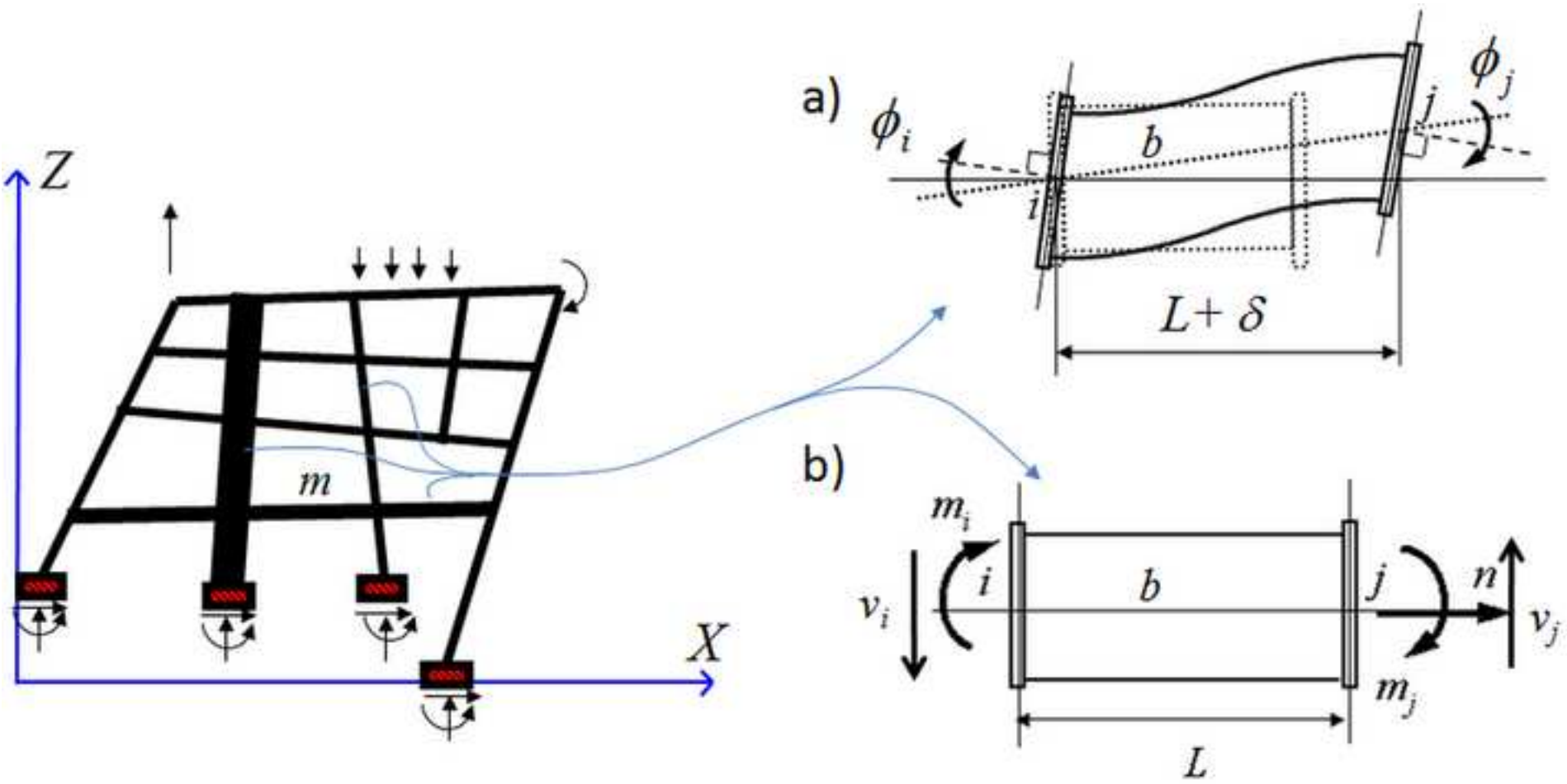

Figure

Click here to download high resolution image

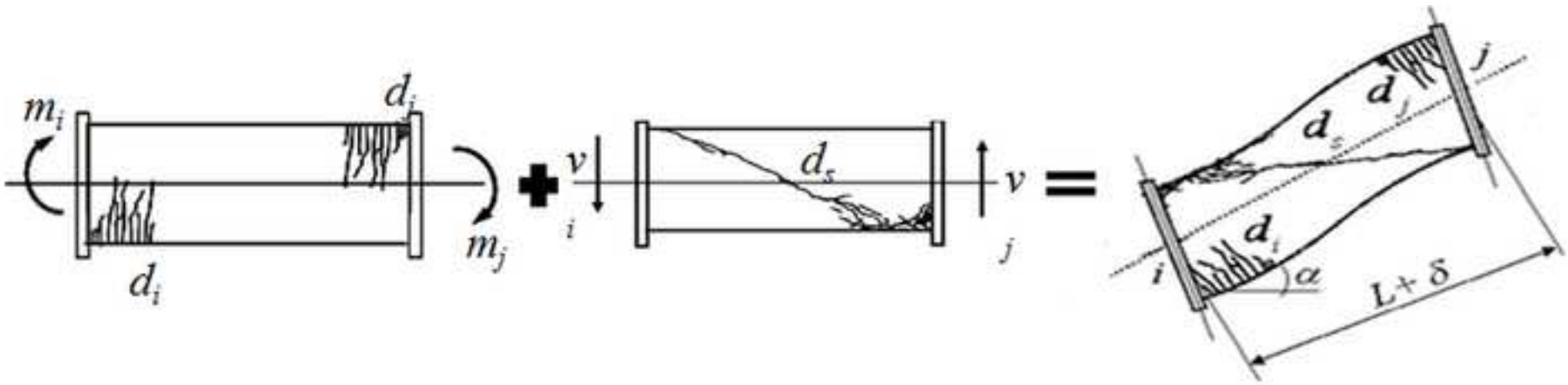

Figure

Click here to download high resolution image

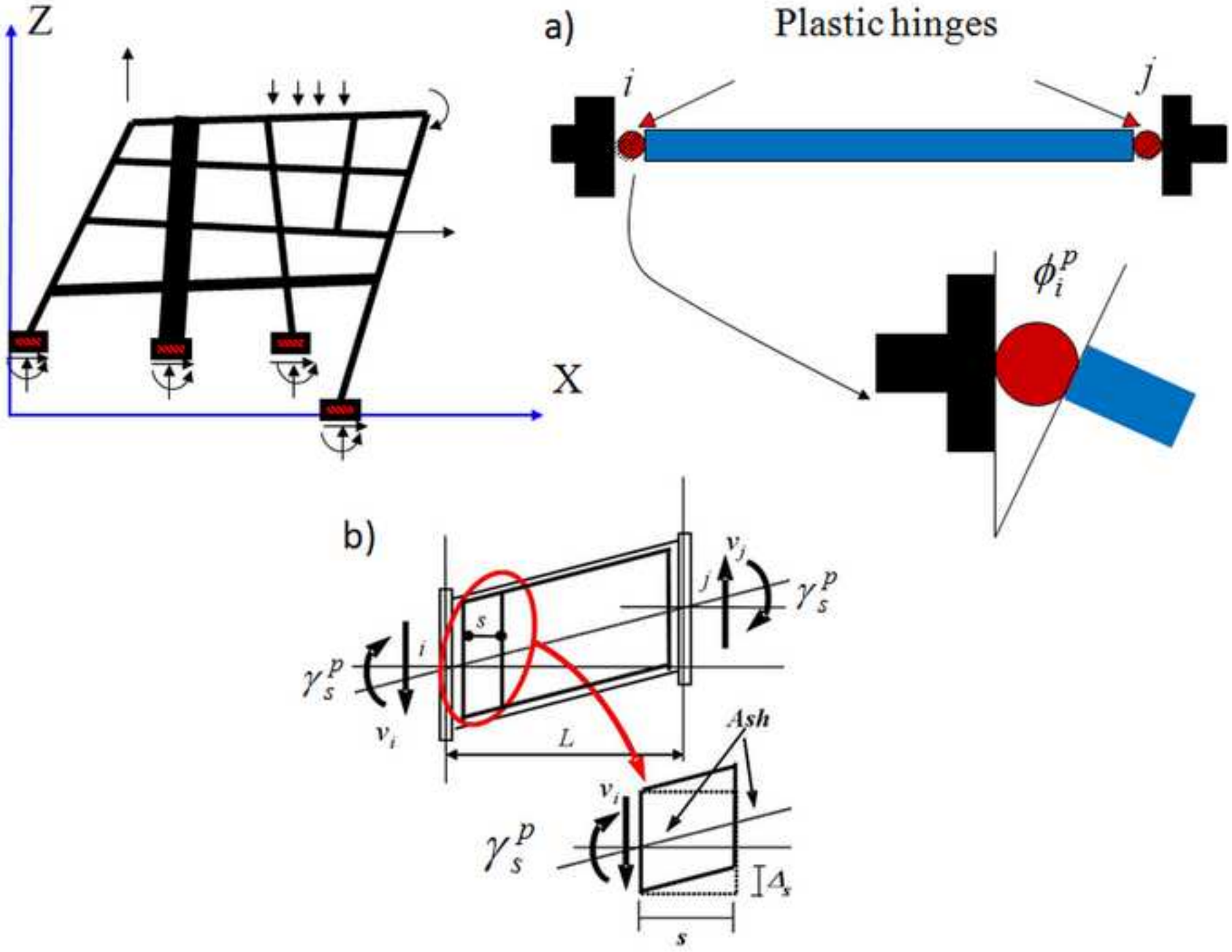

Figure
Click here to download high resolution image

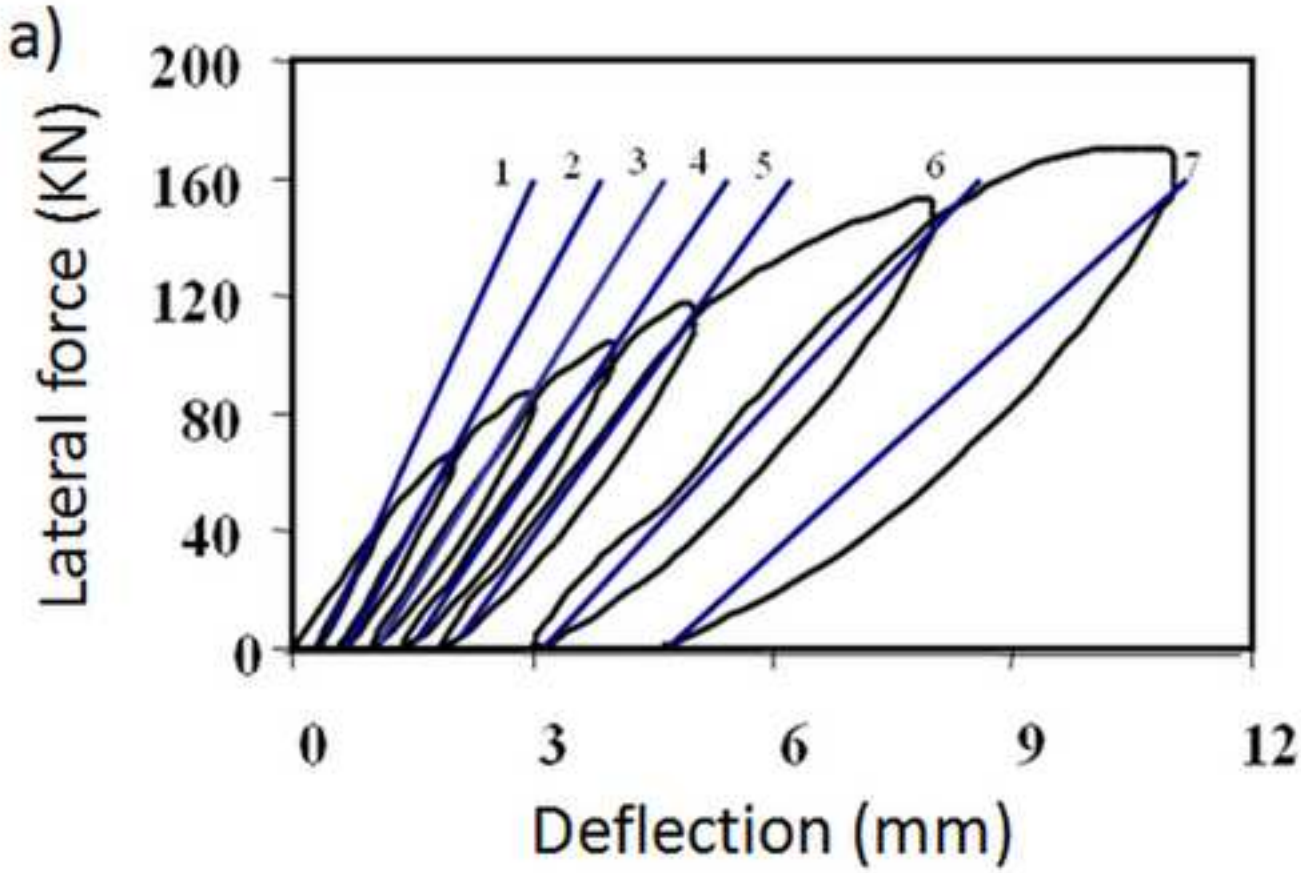

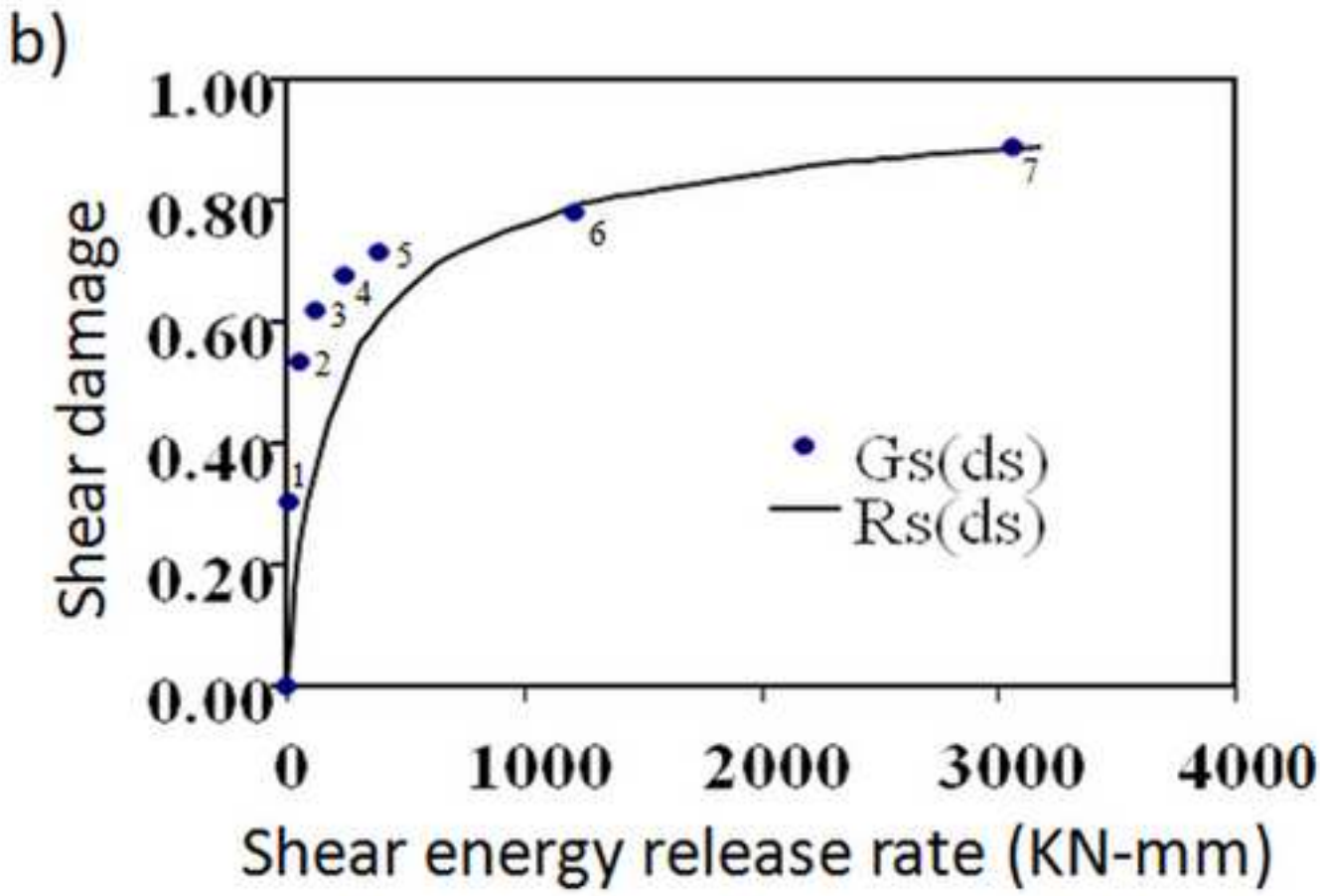

Figure
Click here to download high resolution image

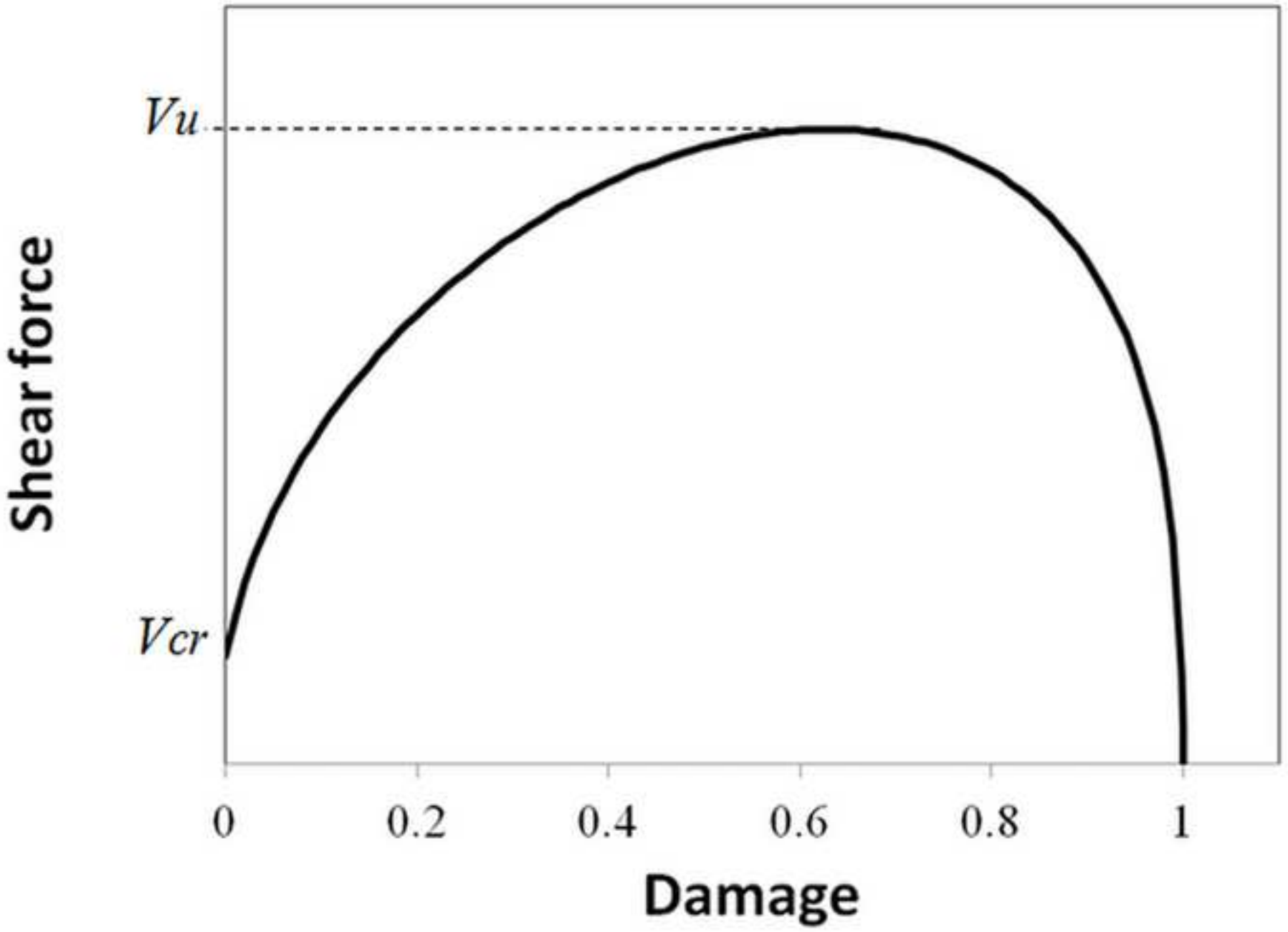

Figure

Click here to download high resolution image

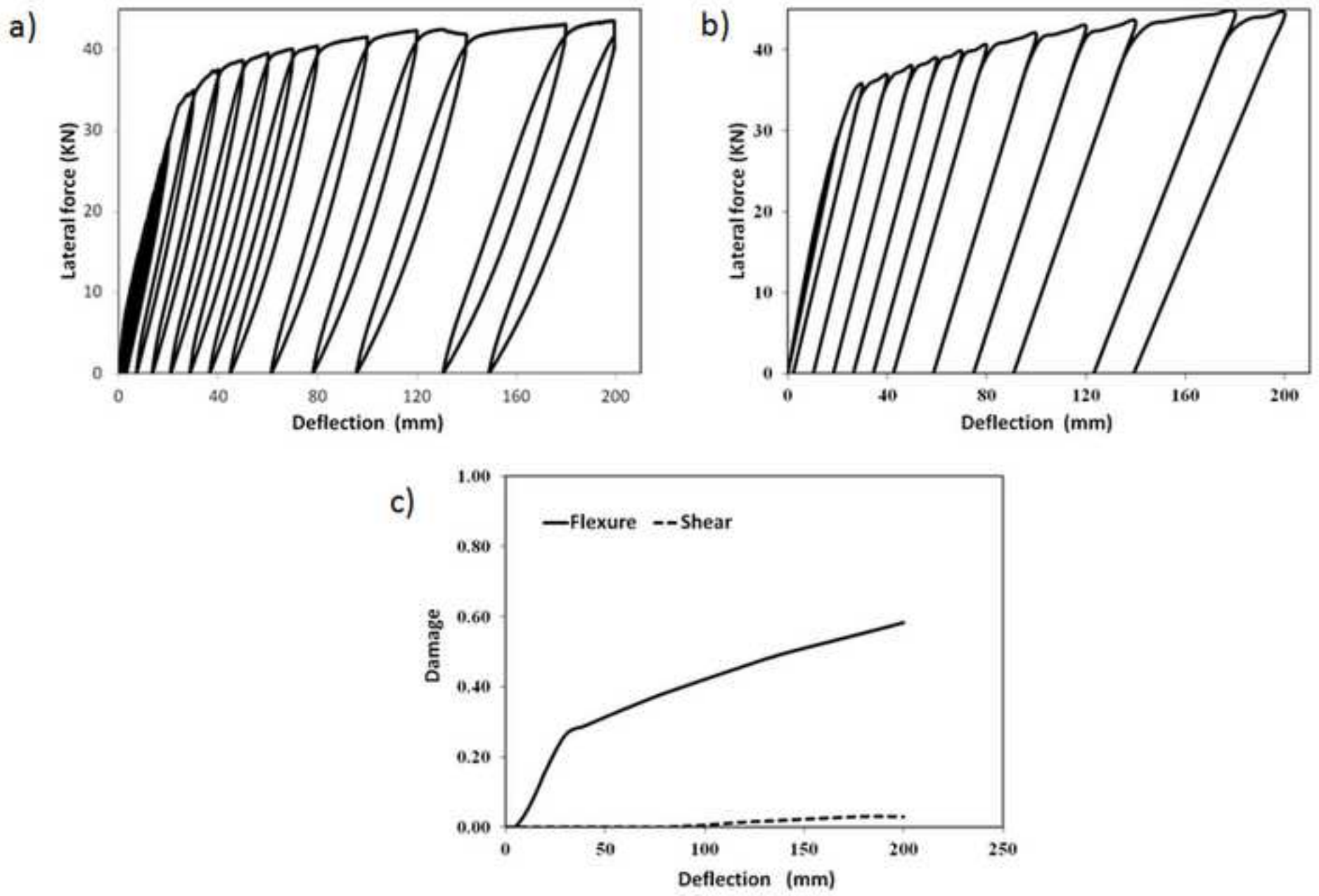

Figure

Click here to download high resolution image

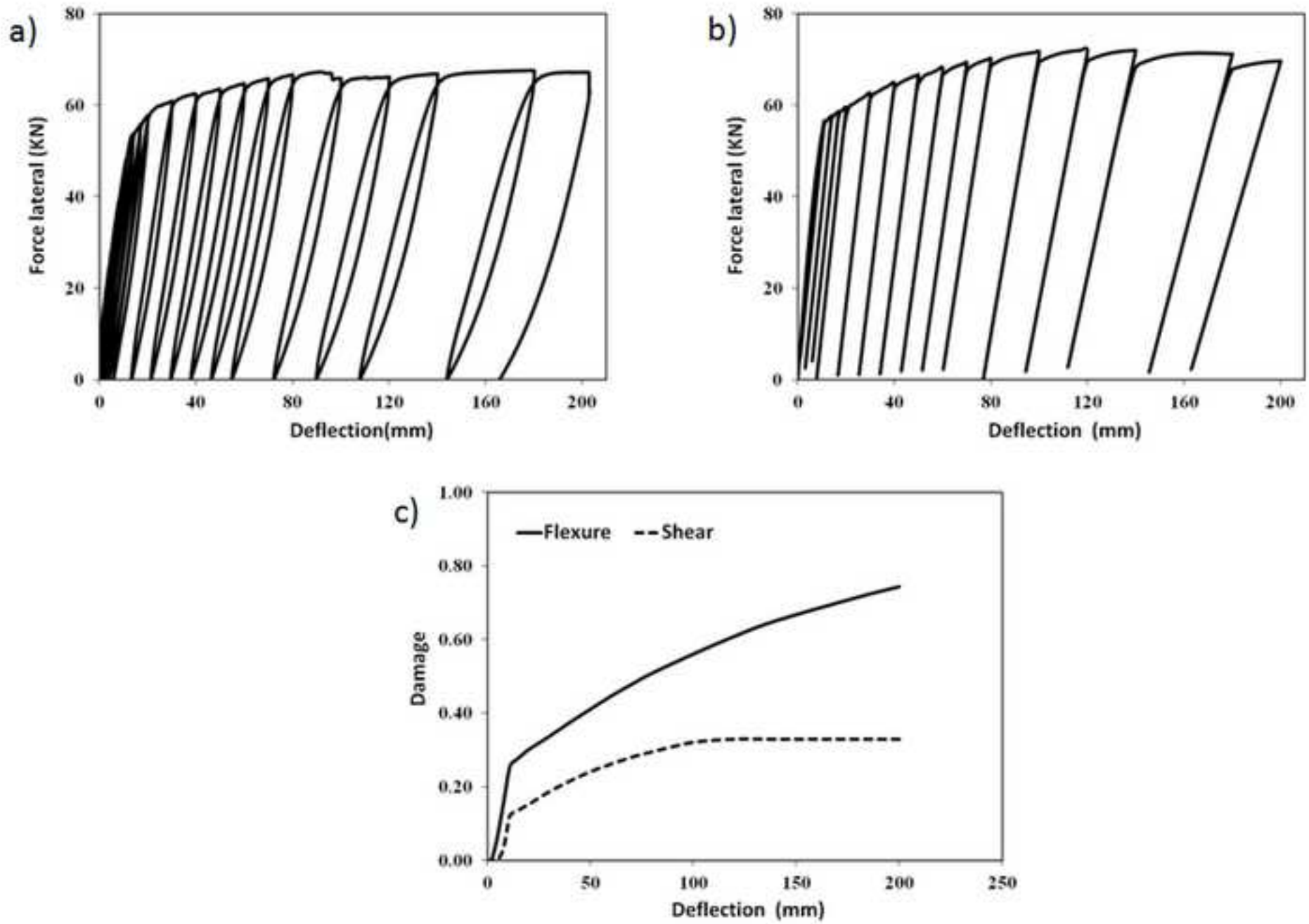

Figure

Click here to download high resolution image

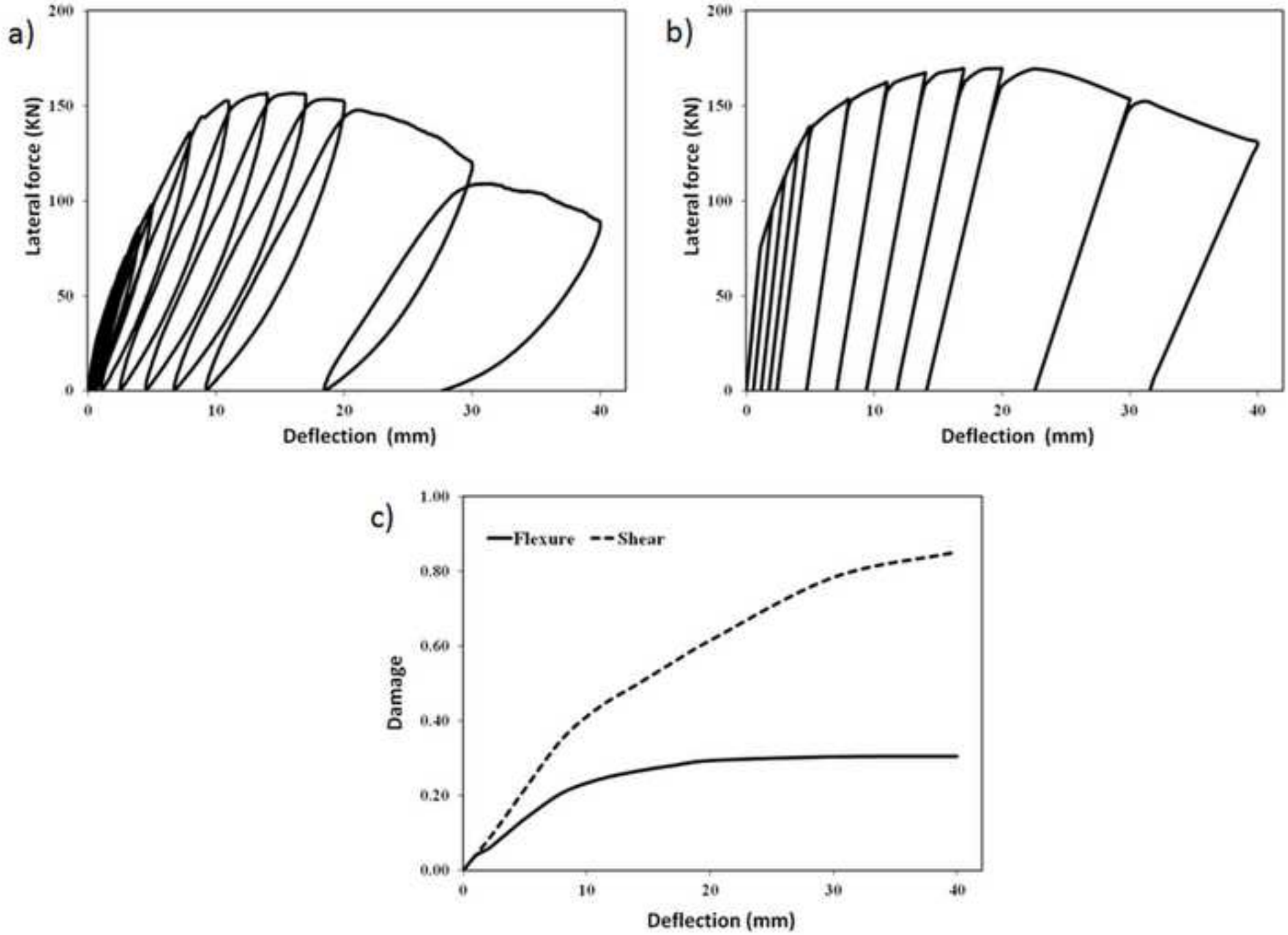

Figure
Click here to download high resolution image

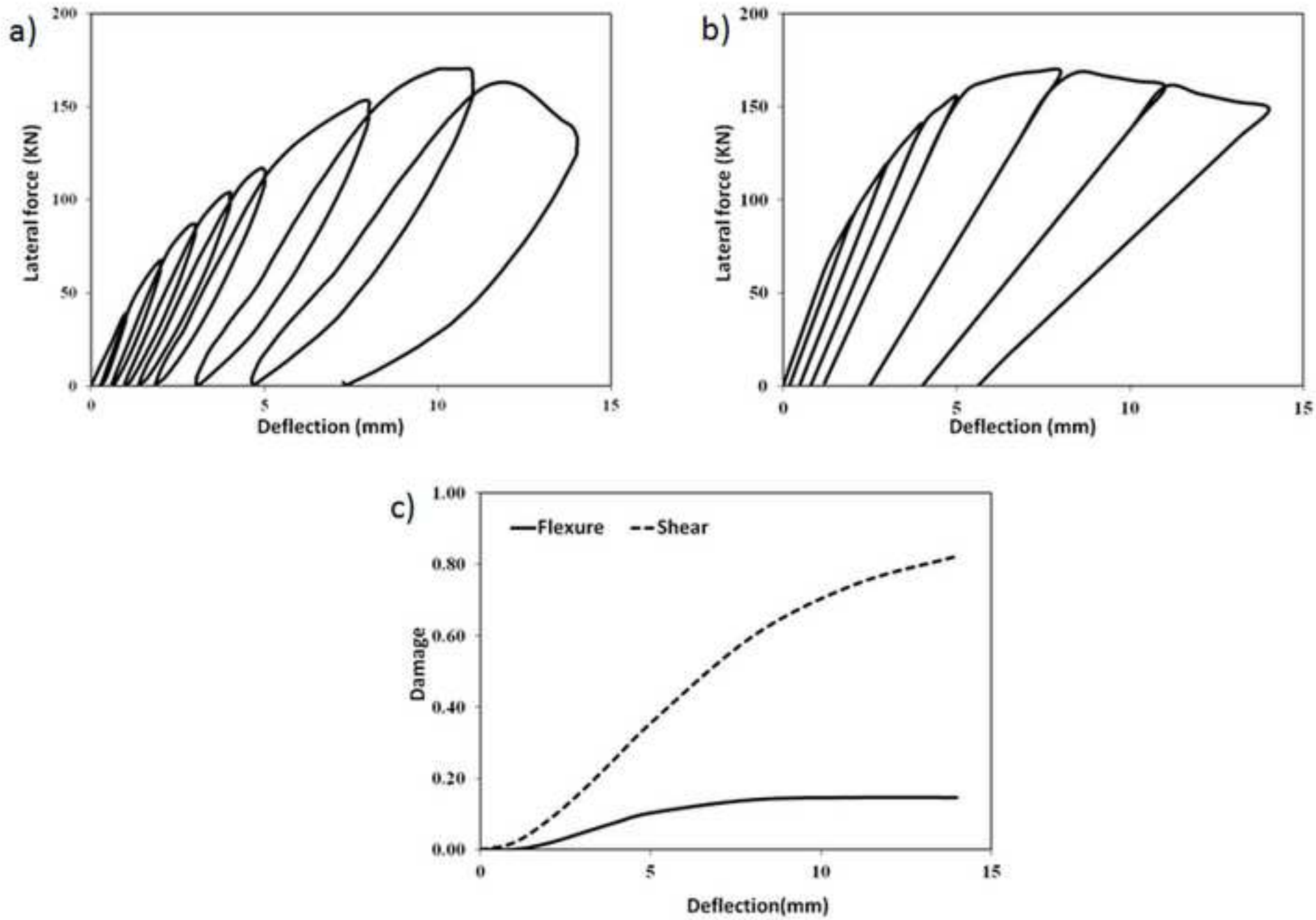

Figure
Click here to download high resolution image

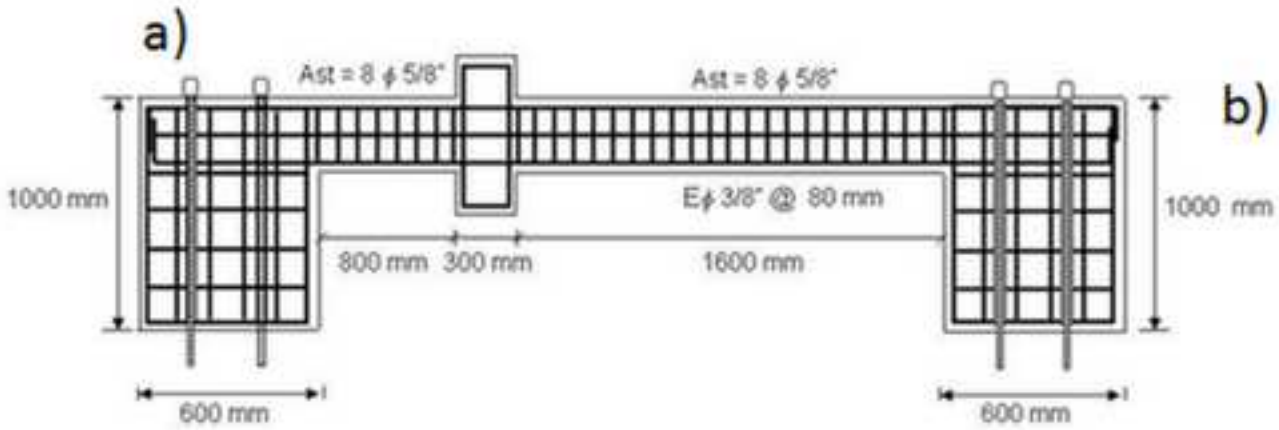

b)

Figure

Click here to download high resolution image

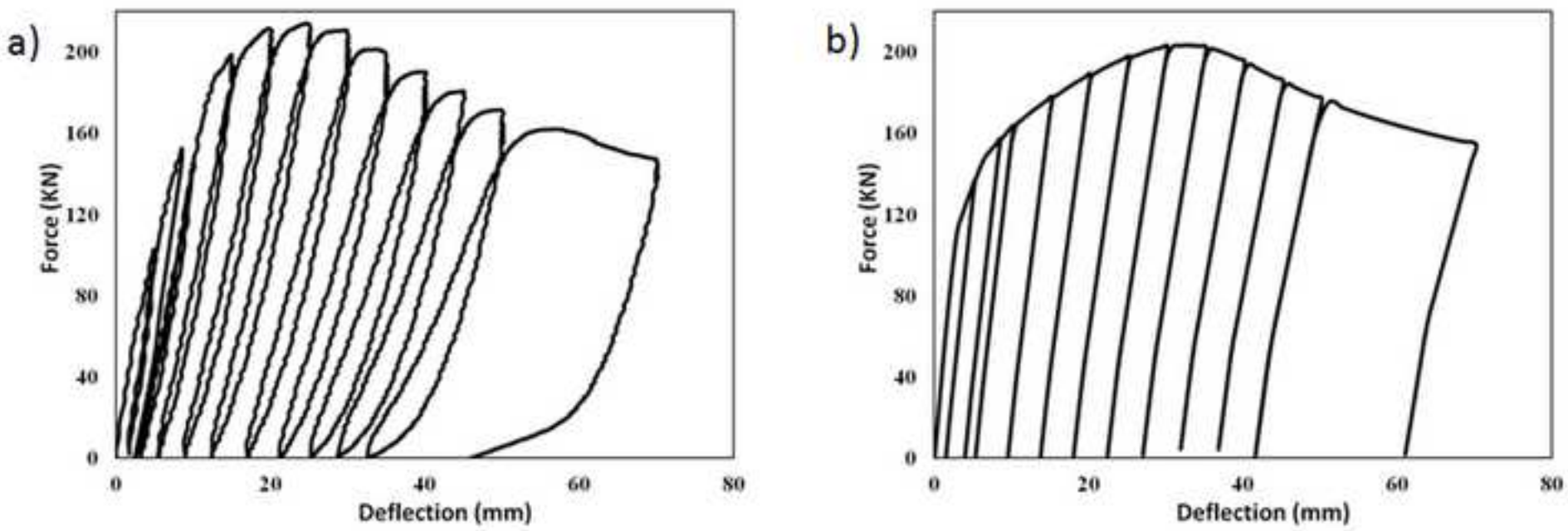

Figure

Click here to download high resolution image